Determining the time constant of the global atmospheric electric circuit through modelling and observations

Rycroft, M. J., Odzimek, A. and Harrison, R. G. ORCID: https://orcid.org/0000-0003-0693-347X (2024) Determining the time constant of the global atmospheric electric circuit through modelling and observations. Journal of Atmospheric and Solar-Terrestrial Physics, 260. 106267. ISSN 1879-1824 doi: 10.1016/j.jastp.2024.106267 Available at https://centaur.reading.ac.uk/116654/

Journal of Atmospheric and Solar–Terrestrial Physics 260 (2024) 106267

Contents lists available at ScienceDirect

Journal of Atmospheric and Solar-Terrestrial Physics

journal homepage: www.elsevier.com/locate/jastp

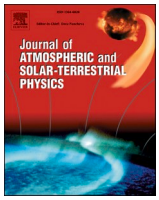

Research Paper

Determining the time constant of the global atmospheric electric circuit through modelling and observations☆,☆☆

Michael J. Rycroft [a], Anna Odzimek [b], R. Giles Harrison [c,*]

[a] CAESAR Consultancy, 35 Millington Road, Cambridge, CB3 9HW, UK
[b] Institute of Geophysics, Polish Academy of Sciences, Ksiecia Janusza 64, 01-452, Warsaw, Poland
[c] Department of Meteorology, University of Reading, Earley Gate, Reading, RG6 6ET, UK

ARTICLE INFO

Handling editor: Dora Pancheva

ABSTRACT

The DC global electric circuit (GEC) distributes charge in the lower atmosphere by current flow between "generator regions" (thunderstorms and rain clouds) and "load regions" (distant conductive air), with a timescale defined by circuit properties. Previously, the load has only been modelled by assuming fair weather (FW) conditions, neglecting cloud. As stratiform clouds cover ~30 % of the Earth's surface, load resistance has been added to represent them, considered to provide semi fair weather (semi-FW) conditions. This increases the GEC timescale by 9 % for stratocumulus, or 33 % for stratus at a lower level. Including mutual capacitance between the outer charged layer and an electrode representing stratocumulus clouds increases the timescale by 35 %, to 8.6 min. These modelled results - the first including the semi-FW aspects - are demonstrated to be consistent with experimentally determined timescales of the real GEC, of between 7 and 12 min, derived from volcanic lightning variations associated with the May 2011 Grímsvötn eruption in Iceland. Accounting for semi-FW circumstances improves the modelled representation of the natural global circuit. Further, the GEC timescale is comparable with cloud droplet charging timescales in the updrafts of extensive layer clouds, suggesting its possible relevance to the microphysical behaviour of stratiform (layer) clouds in the climate system.

1. Introduction

In the last hundred years there has been a developing interest in the topic of the DC global atmospheric electric circuit (GEC). First expounded by CTR Wilson in the 1920s (Wilson, 1921; 1929; Harrison 2020), this has thunderstorms and electrified shower clouds as current generators, with resistive and capacitive elements in both the generator and load parts of the circuit. The circuit links the tops of the generators to the ionosphere and, via that, to the atmosphere far away from the generators, which acts as a load. The current density flowing down through the atmosphere is ~2 pA m^{-2}, so that the total current globally is ~1000 A which was first shown by Schonland (1932), page 29, widely confirmed by later measurements (Mühleisen, 1976). The circuit is completed through the Earth's land and sea surfaces and by point discharge (corona) currents up to the thunderclouds (Wilson, 1924, section II). The ionosphere is thus maintained at a high potential, V ~240–300 kV, with respect to the Earth's surface (Markson, 2007). At the turn of the millennium, Rycroft et al. (2000) reviewed earlier work and introduced an electrical analogue of the circuit. Further, they considered the GEC in relation to both its response to changing activity on the Sun (see Gray et al., 2010; and Price et al., 2015) and to climate change (one expression of which is global warming; see Houghton, 2015).

Our understanding of the DC global electric circuit has improved notably in the last twenty years, as has been summarised in review articles prepared by Aplin et al. (2008), Rycroft et al. (2008, 2012), Siingh et al. (2007, 2011, 2015), Williams (2009) and Williams and Mareev (2014) amongst others. Experimental investigations of its characteristics and applications have increased significantly as novel measurement techniques have been introduced. For example, the possible response of global circuit parameters to earthquake precursors has been investigated by (Harrison et al., 2010, 2014), who introduced the acronym ALICE, Atmospheric Lithosphere-Ionosphere Coupling Exchange, and by Pulinets and Davidenko (2014). The coupling is also discussed by Ouzounov

☆ http://physics.stackexchange.com/questions/187139/capacitance-of-a-single-charged-plate.☆☆ http://physics.stackexchange.com/questions/102076/capacitance-of-bodies-with-different-charge.

* Corresponding autho.
E-mail addresses: michaelrycroft@btinternet.com (M.J. Rycroft), aodzimek@igf.edu.pl (A. Odzimek), r.g.harrison@reading.ac.uk (R.G. Harrison).

https://doi.org/10.1016/j.jastp.2024.106267
Received 8 December 2023; Received in revised form 8 May 2024; Accepted 26 May 2024
Available online 31 May 2024

et al. (2018), as Lithosphere-Atmosphere-Ionosphere Coupling, LAIC. This aspect is also linked to enhanced radon production at the Earth's surface occurring before earthquake precursors (Barbosa, 2020; see also Ponomarev et al., 2011; Golubenko et al., 2020). Hayakawa (2015) has discussed earthquake precursors across the electromagnetic spectrum from the lowest frequencies up to very high frequencies (VHF).

There is also an AC global electric circuit, excited by electromagnetic radiation produced by lightning at frequencies below ~30 Hz, where the wavelength is of the same order as the circumference of the Earth; these are the Schumann (1952) resonances of the spherical Earth-ionosphere cavity. An active research area concerns possible interactions between such electromagnetic waves and human health – see Palmer et al. (2006) and Hunting et al. (2020). The GEC may therefore have practical bio-physical relevance to human society, beyond its established importance in geophysics and solar-terrestrial physics.

The effect of individual lightning discharges on the ionospheric potential was modelled by Rycroft et al. (2007). Rycroft and Odzimek (2010) similarly modelled the (small) effect on the potential of the ionosphere of the Transient Luminous Event (TLE), known as a sprite (Füllekrug et al., 2006), which is generally caused by a large lightning discharge transferring positive charge to ground, termed a +CG flash (see Füllekrug et al., 2019). The strongest intra-cloud (IC) lightning discharges produce Terrestrial Gamma-ray Flashes (TGFs) at the tops of the most energetic thunderclouds. They have been detected by the Atmosphere-Space Interactions Monitor (ASIM) aboard the International Space Station (Neubert et al., 2020), and a major study of these fascinating phenomena has been published by Mailyan et al. (2020). TLEs and theoretical ideas which can explain their observed features have been recently reviewedby Surkov and Hayakawa, 2020.

In this paper we consider the possible values of capacitance in the fair weather regions of the global circuit system in Section 2, and we propose modifications to the equivalent circuit to include the resistance of layer (either stratus or stratocumulus) clouds in the semi fair weather regions (Harrison et al., 2020) in Section 3. In Section 4 we discuss the time constant of the GEC including these new components; as in the model of Haldoupis et al. (2017), the electrosphere is considered to be much lower than its conventional ionospheric altitude. In Section 5, we propose a new model with a mutual capacitance of the stratus cloud layer derived from the measurements and calculations of Harrison et al. (2020). We provide experimental estimates of the time constants of the real GEC in Section 6. Section 7 considers the excitation of the global circuit by volcanic lightning, specifically using observations from Grímsvötn, Iceland, in May 2011. We discuss the results in terms of the physics of the situation in Section 8, including the effects of low-level clouds in relation to global climate (see also Tinsley, 2022). Finally, section 9 gives the main conclusions of the paper.

2. Capacitances in the load part of the global electric circuit

2.1. Equivalent mutual capacitance

Rycroft et al. (2000) presented a diagram of the global circuit and its representation using various electrical components, and typical numerical values of these were shown. In the estimation of the capacitance of the system, C, the scale height of the neutral atmosphere, ~7 km, was used; it is now realised that this is not correct. Nonetheless, the RC time constant of the circuit, i.e. the time taken to discharge to 63% from an initial value, to be discussed fully in Section 4, was estimated to be 200 $\Omega \times 0.7$ F = 140 s, i.e. ~2.3 min. Electrical sources in the atmosphere must continuously replenish the charge which flows around the GEC. They are essential to prevent the circuit from dying out on a time scale of minutes. We know that it does not die out because a downward electric field is always observed in fair weather conditions at the Earth's surface, E_s, of magnitude 100–150 V m^{-1} (Harrison, 2013). This downward electric field, or (with the opposite sign) the potential gradient, varies with geographic location and with Universal Time (UT). The variation with UT in clean air is termed the *Carnegie curve*, discussed in detail by Harrison (2013). The downward field implies a charge density s on the surface

$$s = \varepsilon_0 E_s \tag{1}$$

of −1 nC m^{-2}, or, multiplying by the area of the planet (assuming the Earth radius R_E to be 6370 km), a total charge of $Q_{fw} = -6 \times 10^5$ C in the fair weather regions. If the simple spherical capacitor is regarded as the appropriate model to represent this system, in which inner and outer spherical electrodes can be identified, there would be an equivalent mutual capacitance C of

$$C = \frac{Q_{fw}}{V_u} \tag{2}$$

where V_u is the upper (i.e. outer electrode) potential, assuming that the inner electrode potential is zero. A typical value for the ionospheric potential V is 250 kV (see, e.g., Rycroft et al., 2000), and therefore C can be estimated to be ~2 F, but the fair weather estimate, Q_{fw}, is expected to be an over-estimate as it neglects polar and disturbed weather regions.

2.2. Spherical capacitor considerations

Continuing to explore these quantities, let us first consider the Earth-atmosphere-ionosphere system as a concentric spherical system, in which C can be regarded as the mutual capacitance between the two conducting spheres; the capacitance is given by

$$C = \frac{4\,\pi\,\varepsilon_0}{\frac{1}{a} - \frac{1}{b}} \tag{3}$$

where ε_0 is the electric permittivity of free space, and a and b are the radii of the inner and outer concentric spheres, respectively. For the specific geometry of the Earth-atmosphere system, the inner spherical electrode has the Earth's radius R_E. If the outer spherical electrode is regarded as being at an effective height h above the Earth's surface, the capacitance becomes

$$C = \frac{4\,\pi\,e_0}{\frac{1}{R_E} - \frac{1}{R_E + h}} \approx 4\,\pi\,\varepsilon_0 \frac{R_E^2}{h} \tag{4}$$

from which the effective height of the outer electrode can be found as

$$h \approx \frac{4\,\pi\,\varepsilon_0\,R_E^2}{C} \tag{5}$$

With the C estimated above of 2 F, and R_E also being known, equation (5) provides an estimate of the radial distance between the electrodes, h = 2.3 km. A similar value for h has been given by Haldoupis et al. (2018) who followed a different line of reasoning. However, the approach used here makes no initial assumptions about the typical lifetime of global thunderstorms, as was done by Rycroft et al. (2000). Even if the capacitance is much less than the equivalent fair weather value assumed, h is still likely to be ~1–10 km.

An estimate of h can be arrived at in another way. Rycroft et al. (2007) and Kudintseva et al. (2016) presented empirical models of the atmospheric conductivity profile, $\sigma(z)$, which is due to air ions being formed by cosmic ray and solar ionisation (Golubenko et al., 2020). The profile of potential in the fair weather (FW) region is derived from this by integration with respect to height, z. Using Gauss' Law of electrostatics, Rycroft et al. (2007) also derived the profile of positive charge density in the fair weather (FW) atmosphere. This was found to resemble a decaying exponential with increasing height, z, with a scale height of about 3 km. Thus, it is not unreasonable to take the "upper electrode" to be at a height where the charge density has fallen to a fraction (1/e) of the charge density just above the Earth's surface. This is because a charge distribution which has an exponential decay of charge density

with increasing height, and a scale height H, can be represented by a uniform charge density over a vertical distance of H; the value of that charge density is the value at the height $z = H$. With this value of $h = 3$ km, C is found to be 1.5 F.

These various lines of argument all point to h locating the equivalent upper electrode within the regions of the lower troposphere which contain layer (or layered) clouds, indicating that a more complete system description of the global circuit requires the inclusion of stratiform, or layer, clouds containing both water and ice, e.g., stratus clouds or stratocumulus clouds. Such extensive layer clouds are by far the most abundant clouds on the planet; averaging over a year, they cover about 30% of the planetary surface (Klein and Hartmann, 1993).

It is important to emphasise that the spherical capacitor model is only conceptual. The DC global circuit is a system of electric fields and currents maintained by certain source currents (e.g., arising from charge separation in electrified clouds such as thunderclouds and electrified shower clouds) in a medium with variable non-zero conductivity. Therefore, the structure and behaviour of the real global circuit is in many aspects substantially different from that implied by the simple electrostatic capacitor models because the region between the electrodes is filled with an inhomogeneous leaky dielectric, of resistivity $\rho(z) = 1/\sigma(z)$, as was discussed by Uman (1974). Indeed, the most natural way to discuss the global circuit is to represent it as a distributed current network rather than as a capacitor. This approach to discussing and modelling the global electrical system has been used since the paper by Holzer and Saxon (1952). More recent models of the DC global circuit are also based on this representation, and they solve equations for the electric potential in a distributed conductive medium (see, e.g., Rycroft et al. (2007), Odzimek et al. (2010) and Bayona et al. (2015), amongst others).

2.3. Layer cloud capacitances

Harrison et al. (2020) have demonstrated that a new component present in the return part of the GEC consists of extensive layer clouds such as stratus (St), which cover about 30% of the Earth's surface. Typically, this is a layer of semi fair weather (SFW) clouds at heights between 0.8 and 1.2 km, a layer $d = 0.4$ km thick, where the conductivity is reduced below the value found in surrounding cloud-free air to 10^{-14} S m^{-1}. Due to the current flowing down through these clouds, the cloud tops, of area A, are charged positively and the cloud bases, also of area A, are charged negatively. They therefore constitute a capacitance whose value is given by standard electrostatics theory as

$$C_{SFW,St} = \varepsilon_0 \frac{A}{d} = \varepsilon_0\ 0.3\ \mathrm{x}\ \frac{4\,\pi\,R_E^2}{400}\ \ \mathrm{F} \tag{6}$$

Inserting numerical values $C_{SFW,St} = 3.39$ F. Calculated in a similar way, the capacitance of the layer below the stratus cloud is 1.69 F, and above up to 3 km is 0.75 F.

Alternatively, we may consider a higher stratocumulus (Sc) cloud, say between 2 and 3 km (see, e.g., Rycroft et al., 2012, fig. 10), so that the thickness of the cloud layer $d = 1000$ m. Here, again, the electrical conductivity is reduced below the value, found in cloud-free air at the same height, to $\sigma = 10^{-13}$ S m^{-1} (see, e.g., Aplin et al., 2008; Kudintseva et al., 2016). They therefore constitute a capacitance whose value is given by

$$C_{SFW,Sc} = \varepsilon_0 \frac{A}{d} = \varepsilon_0\ 0.3\ \mathrm{x}\ \frac{4\,\pi\,R_E^2}{1000}\ \ \mathrm{F} \tag{7}$$

Inserting numerical values, $C_{SFW,Sc} = 1.35$ F. The capacitance of the air below the cloud is 0.68 F.

We now consider the situation when we have a cloud-free atmosphere over ~70% of the Earth and low altitude clouds over the remaining 30%. The capacitances representing these two regions are taken to be C_1 and C_2, respectively; they are in parallel so that the total capacitance of the system is

$$C = C_1 + C_2 \tag{8}$$

which, as discussed above, has the value ~1.5 F (see also the Appendix). The fair-weather capacitance C_1 has the value $0.7 \times 1.5 = 1.05$ F, and this is shown as C_{FW} in the new circuit diagram, Fig. 1. Also shown in Fig. 1 are the capacitances of the semi fair weather atmosphere from the ionosphere down to the top of the cloud, and from the ground up to the bottom of the cloud, for which the numerical values are calculated following similar procedures to those above. The total capacitance of the series of capacitances in the semi fair weather area from ground level through the cloud area up to the level h is equal to $C_2 \sim 0.3 \times 1.5 = 0.45$ F.

3. Resistances in the load part of the global electric circuit

3.1. General expression for resistance of a column of air

A careful and thorough analysis of the charge distribution in the entire DC global circuit must be based upon either numerical modelling of the entire global circuit or its representation in the form of a multi-column electric network. Here we shall proceed following the latter path.

For comparison with our earlier results, and for simplicity, we specify the ionospheric potential to be 250 kV, and the total current flowing around the GEC to be 1.0 kA. It is worth noting that Peterson et al. (2017) show, from satellite observations, that the total current is between 1.4 and 1.6 kA.

The resistance of the entire atmosphere remote from the generators (which occupy a negligible proportion of the Earth's surface area), R, is in general given by

$$R = \frac{1}{4\,\pi\,R_E^2} \int_{z=0}^{z=h} \rho(z)\,dz, \tag{9}$$

where $\rho(z)$ is the resistivity profile or, in terms of the conductivity profile $\sigma(z)$, by

$$R = \frac{1}{4\,\pi\,R_E^2} \int_{z=0}^{z=h} \frac{dz}{\sigma(z)} \tag{10}$$

Here, h is the height of the outer electrode, which is usually taken as being the ionosphere. Beginning at ~60 km altitude and going up to the ionosphere is the electrosphere, where the electrical conductivity is so large that the layer is essentially at a constant electric potential. So, h is also approximately the height of the electrosphere.

Model estimates for the global resistance are about 200–250 Ω (Makino and Ogawa, 1984; Tinsley and Zhou 2006; Baumgaertner et al., 2013). Such a value for this resistance was set by Rycroft et al. (2000) as 200 Ω and by Rycroft et al. (2007) and Rycroft and Odzimek (2010) as 250 Ω. In the current model we distinguish between the resistance of the semi fair weather containing the low cloud layer, and the remaining semi fair weather and fair weather resistance. In addition to the resistance of solely the fair weather region, this would include the resistance through high and mid-level clouds, which are generally less than that of low level clouds, either because of reduced cloud thickness or greater conductivity inside the cloud at a higher altitude.

3.2. Cloud layer resistance

Zhou and Tinsley (2010) calculated vertical conductivity profiles through clouds of various types and estimated their contribution to the global resistance. Their calculations give a range of values for the total resistance from 192 Ω to 237 Ω, depending on season, with the decrease of the within-cloud conductivity from ~1/60 to ~1/20 of the

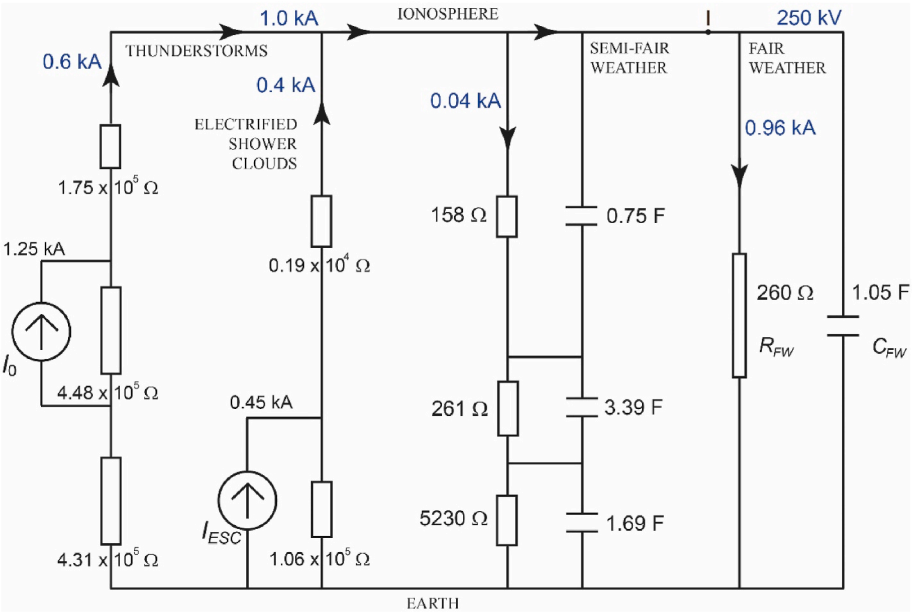

Fig. 1. Schematic diagram of the global electric circuit (based on Rycroft et al., 2007, fig. 12; see also Rycroft and Odzimek 2010, Fig. 1) with ~70% of fair weather area and 30% of semi fair weather area covered by stratus clouds at an altitude between 0.8 and 1.2 km.

conductivity of cloud-free air at the same level. The cloud-free air conductivity over the oceans is estimated as $\sim 3 \times 10^{-14}$ S m^{-1}, and, over the continents, from 2×10^{-13} S m^{-1} at the Antarctic plateau to $\sim 1 \times 10^{-14}$ S m^{-1} at mid-latitude sites (Tinsley and Zhou 2006, fig. 10), and less in the more polluted regions. Tinsley and Zhou (2006) provide spatial estimates of the conductivity with polluting aerosol variations considered, also allowing for reduced ion production over the oceans. Kubicki et al. (2016) have investigated the effect of varying concentrations of aerosols, with sizes less than 1 μm, on the vertical electric field at ground level observed at three stations at different latitudes. Anisimov et al. (2020) have shown the results of model calculations of variations of the concentrations of aerosols of different sizes with height in the planetary boundary layer (PBL). The presence of any aerosols, tiny droplets and particles which are much larger than molecules, and pollution of the atmosphere near the Earth's surface, significantly reduce the conductivity of the air (see also Harrison 2006; Tacza et al., 2020).

Following equation (10), integration of the inverse of the conductivity (i.e. resistivity) profile over a range of altitudes and dividing by the surface area, A, yields the resistance of the air and cloud layers occupying portions of the atmosphere for the specified altitude range and for the surface area equal to A. Alternatively, an average conductivity for the height range can be used, multiplied by the difference between the heights, d, and divided by the surface area A.

For the stratus (St) cloud of thickness d between heights of 800 and 1200 m, where the conductivity is taken to be 10^{-14} S m^{-1} (Harrison

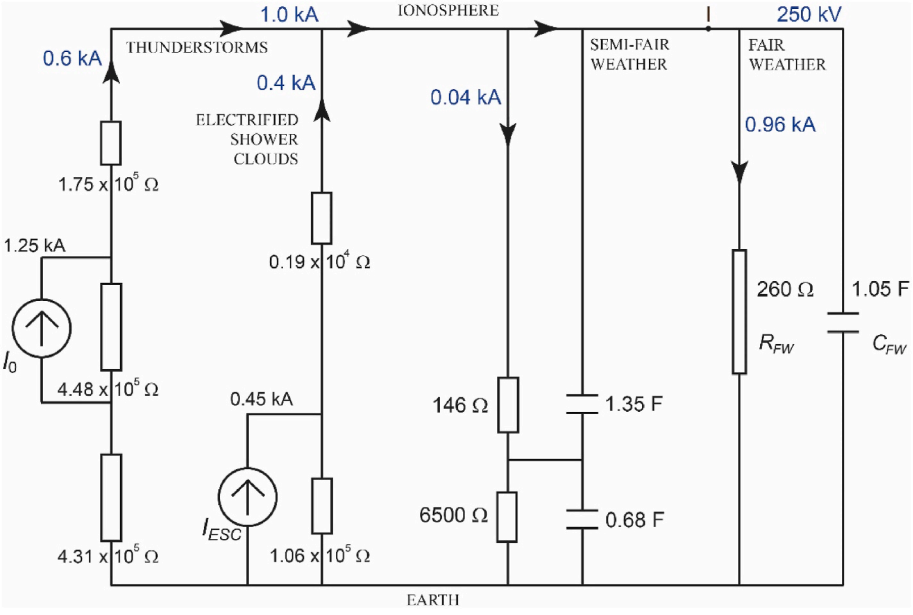

Fig. 2. Schematic diagram of the global electric circuit with ~70% of fair weather area and 30% of semi fair weather area covered by stratocumulus clouds, considered to be at an altitude between 2 and 3 km, which sets the altitude of the upper plate of the C_{SFW}. The resistances of the cloud layer and above the cloud layer have been merged into one.

et al., 2020), the resistance of the cloud layer covering 30% of the Earth's surface, represented as a flat plate of area A, is

$$R_{SFW,St} = \frac{d}{A\,\sigma} = \frac{400}{0.3\;4\,\pi\,R_E^2\;\;10^{-14}} = 261\ \Omega \tag{11}$$

If these semi fair weather (SFW) clouds were present over the entire Earth, the results given by Eq. 4.12 in the paper by Harrison et al. (2020) can be used to estimate the change in the GEC resistance. These require that the proportional increase of resistance should be by (2.00–1.74)/2.00 = 0.13, i.e. an increase of 13%.

Returning to the case of a stratocumulus (Sc) cloud between heights of 2 and 3 km (Fig. 2), we consider that the conductivity of the cloud layer at this height is $\sigma = 10^{-13}$ S m^{-1}, so that the resistance of this cloud layer is

$$R_{SFW,Sc} = \frac{d}{A\,\sigma} = \frac{1000}{0.3\;4\,\pi\,R_E^2\;\;10^{-13}} = 65\ \Omega \tag{12}$$

We also need to estimate the resistance of the planetary boundary layer up to the lower edge of these stratiform clouds. This is difficult to estimate reliably because it is so variable in both space and time; this is because the concentration of aerosols in the air near the Earth's surface is so variable, on at least daily timescales, as mentioned by Harrison et al. (2020). Table 3 of Odzimek et al. (2018) shows that the air conductivity below mid-latitude land stratus clouds (without precipitation, i.e. rain or snow) is $< 2 \times 10^{-15}$ S m^{-1}; let us take 10^{-15} S m^{-1}. Thus, the resistance of the planetary boundary layer under the stratus (St) clouds covering 30% of the Earth's surface is

$$R_{PBL,St} = \frac{800}{0.3\;4\,\pi\,R_E^2\;\;10^{-15}} = 5230\ \Omega \tag{13}$$

Under the stratocumulus (Sc) clouds, the resistance of the planetary boundary layer is a little greater, say

$$R_{PBL,Sc} = 6500\ \Omega \tag{14}$$

Also shown in Figs. 1 and 2 are the resistances of the semi fair weather atmosphere from the ionosphere down to the top of the cloud. The numerical values for the two types of cloud, St and Sc, are found from Fig. 5 of Rycroft and Harrison (2012) which plots the percentage of the fair weather columnar resistance up to 10 km altitude as a function of height. Only 7% of the total columnar resistance is at heights above 10 km. Therefore, the resistance from the ionosphere down to the 10 km level is 0.07 × 260 Ω, which is 18 Ω; the resistance below 10 km is 242 Ω.

From the 10 km level down to the top of the stratus cloud, at a height of 1.2 km, Fig. 5 of Rycroft and Harrison (2012) shows that the resistance is (100–42) % = 58 % of 242 Ω = 140 Ω. From 10 km down to the top of the stratocumulus cloud, at a height of 3 km, the resistance is (100–74) % = 26 % of 242 Ω = 63 Ω. The resistances down from the ionosphere to the cloud top shown in Fig. 1 (stratus) and Fig. 2 (stratocumulus) are, respectively, (18 + 140) = 158 Ω and (18 + 63) = 81 Ω.

3.3. Fair weather resistance

Calculation of the pure, cloudless, fair weather resistance can be achieved following two ways of reasoning. One option is to consider the new fair weather resistance as an area-wise share of the total resistance, i.e. 70 % of 250 Ω which gives 175 Ω. Another is to keep the effective semi and fair weather resistance at 250 Ω. We shall apply the second option, keeping the fair weather resistance constant at 250 Ω, as this allows us to retain the ionospheric potential at 250 kV and the total current at 1 kA. Considering the large values of resistance of the cloudy semi fair weather in parallel with pure fair weather, the value of the resistance of the latter needs to be only slightly increased to 260 Ω.

The addition of the capacitances and resistances, representing the semi fair weather clouds around the world, to the electrical engineering analogue model of the GEC (Rycroft et al., 2007) is presented in the centre of Fig. 1. Numerical values of the components for the stratus model of Harrison et al. (2020) are shown. Compared to the analysis of Rycroft et al. (2007), in order to investigate the time constants of the fair-weather area, we have not included the capacitances aligned with the resistances in the generator areas: thunderstorms and shower clouds. This further simplifies the situation and allows us to compare the new time constants with the RC time constant 250 Ω × 1.5 F = 375 s of the fair weather circuit, when the layer clouds are not specifically distinguished.

It is noteworthy that the proportion of the return current flowing through the extensive layer clouds is very small compared with the fair weather current (~4%). This is because the resistance of the PBL below the clouds is so large, compared with the other resistances in the return part of the GEC.

3.4. Differences between stratus clouds over oceans and continents

Allowing for differences between continental and ocean stratus affecting the resistances in the circuit and noting that a large part of the stratus coverage lies over the oceans, we investigate this issue in more detail. We use the simplified model conductivity profiles of Makino and Ogawa (1985) for continental air (surface aerosol concentrations of 10000 particles cm^{-3}) and oceanic air (sea-level aerosol concentrations of 1000 particles cm^{-3}), including the reduced conductivity within clouds. However, to account for the differences between land and sea more realistically, rather than assuming the uniform cloud parameters of Makino and Ogawa (1985), such as the cloud particle concentration (N_c = 200 cm^{-3}), we follow instead the method of Zhou and Tinsley (2010) and use the cloud parameters of Hess et al. (1998). Different cloud particle concentrations for maritime and continental stratus, of N_c = 80 and N_c = 250 cm^{-3} respectively, are considered (Hess et al., 1998, Table 1a), with a uniform ion attachment coefficient $\beta_c = 10^{-3}$ cm^3 s^{-1}. Calculated conductivity profiles with these assumptions are shown in Fig. 3. According to these calculations the sea-level value of the air conductivity is taken to be 1.6 × 10^{-14} S m^{-1}, and ground-level air conductivity equals 5.0 × 10^{-15} S m^{-1}.

The columnar resistance, R_c, through the layers is 2.0 × 10^{17} Ω m^2 over the oceans and over land 3.3 × 10^{17} Ω m^2, assuming that the equalising potential layer is at 3 km. For the stratus (St) cloud of thickness d between heights of 800 and 1200 m, the integration of the conductivity inverse gives the cloud resistance $R_{SFW,St}$ = 1095 Ω over the

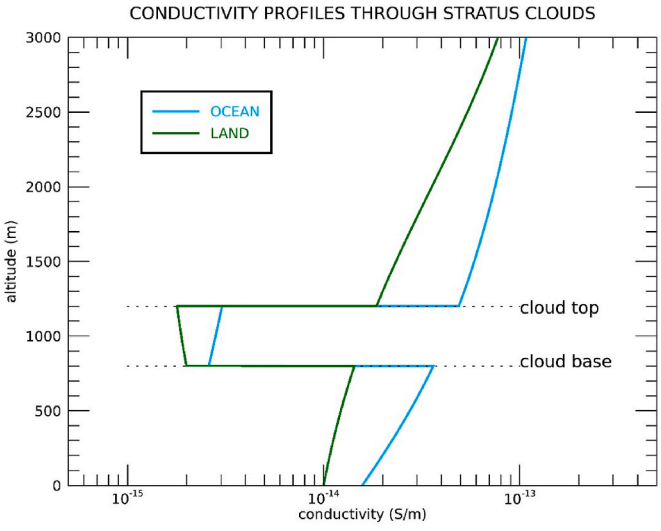

Fig. 3. Conductivity profiles through land and ocean stratus clouds, calculated according to Makino and Ogawa (1985) with the cloud properties of Hess et al. (1998).

oceans, and 9245 Ω over land. The resistances below the cloud amount to 259 Ω over the oceans and 2980 Ω over the land, and the resistances from the cloud top up to 3.0 km are 187 Ω and 2240 Ω, respectively (Fig. 4). The remaining fair and semi fair weather resistance needs to be adjusted to 305 Ω to keep the total resistance of 250 Ω. A smaller fraction of the total current, 0.16 kA, flows through the ocean stratus layer, and only about 20 A through the stratus layer over the land.

4. Time constant of the global electric circuit

Price et al. (1997) consider that the timescale λ over which the Earth maintains its negative charge, by drawing on the fair-weather electric current $I_{FW} \sim 1250$ A (Rycroft et al., 2000), is given by

$$I_{FW} = \frac{dQ}{dt} \sim -\frac{Q}{\lambda} \tag{15}$$

so that $\lambda \sim -Q/I_{FW} = 2 \times 10^5$ C/1250 A = 160 s.

We can estimate the time constant in another way. Using the values given by Rycroft et al. (2007), $R = 250$ Ω. This resistance is in parallel with the capacitance of the fair weather atmosphere, $C_{FW} \sim 0.5$ F, so that the time constant of the global circuit τ is $RC \sim 125$ s. However, taking the value $C_{FW} = 1.5$ F estimated in Section 2, the time constant is increased threefold to ~375 s (6.3 min). With the new values for the fair weather part of the circuit introduced in this paper and shown in Figs. 1 and 2, the RC time constant τ in the pure fair weather would be 260 × 1.05 = 273 s (4.5 min). As with the model of Haldoupis et al. (2017), the outer electrode of the GEC, the electrosphere, is considered to be at an extremely low altitude, just below ~3 km.

The time constants in the fair weather part of the circuits shown in Figs. 1 and 2 are the same as the time constant of the change of the fair weather current or the ionospheric potential, i.e., the electric potential of node "I". This can be determined as the time after which the ionospheric potential V_I of 250 kV decreases to the level $V_I/e \sim 92$ kV in response to abruptly switching off the circuits' generators. Simulations made with OrCAD PSpice software give the following time constants: 497 s (8.2 min) when stratus clouds covering 30% of the Earth's surface are present, and 407 s (6.8 min) when stratocumulus clouds are present. The GEC time constant of this revised global circuit model is 33% or 9%, respectively, greater than the original RC time constant of 375 s (6.3 min). This time constant is longer than the original time constant due to additional capacitances in the remaining parts of the circuit to which R_{FW} is connected, namely the C_{SFW} capacitance of the semi fair weather area of the circuit. When land and ocean stratus are considered as in Section 3, this time constant is 480 s (8 min).

5. Mutual capacitance of two charged plates for the stratus cloud

For the consideration of the parallel plate capacitance to apply, the electric field between the plates is taken to be spatially uniform and temporally constant. This is purely an electrostatic situation, as mentioned in Section 2; the atmospheric situation will be different, because of mechanical (e.g., turbulent) processes which lead to charge transfer. For the solely electrostatic situation, electric charge is stored on each of the two plates, positive charge on the upper plate at a potential of V_U and negative charge on the lower plate at a potential of V_L.

We can consider the upper plate of the stratus cloud model at a height of 1.2 km to have a capacitance to Earth of C_U and the lower plate, at a height of 0.8 km, a capacitance to Earth of C_L. There will be a mutual capacitance to Earth, C_M, between them as indicated in Fig. 5. There is a standard expression[1] for the capacitance of an isolated disk of radius R, which is $8\,\varepsilon_0\,R$. For a disk having an area of 0.3 times the Earth's surface area,

$$R = 0.3^{0.5} R_E = 0.548\,R_E = 3490 \text{ km}, \tag{16}$$

so that

$$C_U = C_L = 2.47 \times 10^{-4} \text{ F}. \tag{17}$$

We now use the result[2] that the charges on the upper and lower plates are, respectively, $Q_U = C_U\,V_U + C_M\,(V_U - V_L)$ and $Q_L = C_L\,V_L + C_M\,(V_L - V_U)$. From Fig. 5c of Harrison et al. (2020), which shows the potentials and charges on the upper plate, Q_U is given by:

$$Q_U = 1.28 \bullet 0.3 \bullet 4\pi\,R_E^2 = 2.75 \times 10^5 \text{ C} \tag{18}$$

From Fig. 6 of Harrison et al. (2020) which gives the potentials, $V_U \sim 80$ kV and $V_L \sim 35$ kV, we find that

$$Q_U = 2.47 \times 10^{-4} \bullet 8.0 \times 10^4 + C_M \bullet 4.5 \times 10^4 \tag{19}$$

and that

$$Q_L = 2.47 \times 10^{-4} \bullet 3.5 \times 10^4 - C_M \bullet 4.5 \times 10^4 \tag{20}$$

Therefore,

$$Q_U = 19.8 + 4.5 \times 10^4\,C_M = 1.96 \times 10^5\,C \tag{21}$$

Here, the value close to 20 C is negligible compared with the value of almost 200,000 C, so that:

$$C_M = \frac{Q_U}{V_U - V_L} = \frac{19.6}{4.5} = 4.36 \text{ F}. \tag{22}$$

In Fig. 5, such a mutual capacitance derived from the observed charges replaces the capacitance representing the stratus cloud layer in Fig. 1. The self-capacitances (to Earth) are also included. From the PSpice simulations the time constant is about 499 s (8.3 min), which is a 35% increase from 375 s, and a similar result to the previously analysed stratus case in Fig. 1.

6. Experimental determination of the global circuit time constant

Whichever model is used, the increase in the time constant of the modelled GEC from its original value of 260 s is rather small, <40%. It may therefore be difficult, using observations of atmospheric electricity quantities, to distinguish between them. In principle, determining the time constant of the actual GEC requires either a perturbing influence, to which a subsequent response can be defined, or by analysis of the power spectrum which emerges following the filtering effect of the global circuit. An appropriately major perturbing influence could be the atmospheric ionisation caused by a nuclear weapon, a solar flare, a ground level event (GLE, see, e.g., Cohen and Mewaldt, 2018; Golubenko et al., 2020), a gamma-ray burst (see Brown, 1973; Inan et al., 1999) or a period of enhanced lightning with an implied increase in the input current to the global circuit. In any of these cases, rapid time response measurements of the potential gradient or conduction current density are needed to determine the timescale of the response.

Some volcanic eruptions have generated appreciable and identifiable transient increases in lightning. For example, the eruption of the Icelandic volcano Grímsvötn during May 2011 produced substantial volcanic lightning (Fig. 6a), which occurred in several periodic pulses (Fig. 6b), attributed to resonances in the magma chamber beneath (Arason et al., 2012). Around midnight UTC on May 21, 2011, when, globally, lightning is approaching its daily minimum, Fig. 4c shows that the Grímsvötn eruption provided a major source (~20%) of the global lightning fixes that were determined by the UK Met Office's Arrival Time Detection (ATD) lightning monitoring system (Bennett et al., 2011; Lee, 1986). For the ATD system, the threshold lightning current for detection over Iceland at that time was 3 kA (Aplin et al., 2016).

At Reading, which had undisturbed weather from May 21, 2011 until a brief rain shower around 04 UTC on 22nd May, measurements were made of the potential gradient (PG) and the current flowing to an isolated flat plate. In the PG data, a pulse is evident around the same time as the lightning pulse, suggesting an association between them (Fig. 6d).

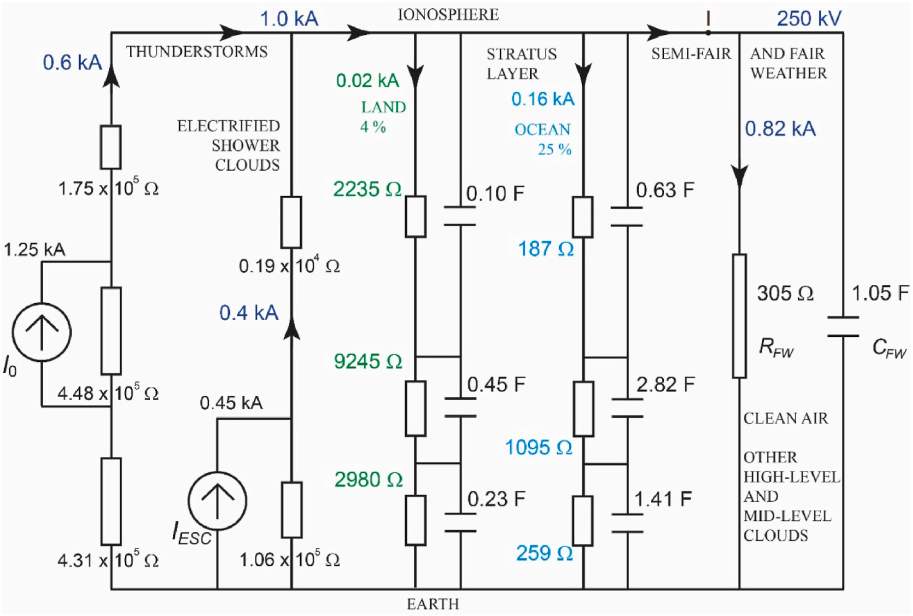

Fig. 4. Schematic diagram of the global electric circuit with ~70% of fair and semi fair weather area and 30% of semi fair weather area covered by stratus clouds at an altitude between 0.8 and 1.2 km, over land (4%) and over the oceans (25%).

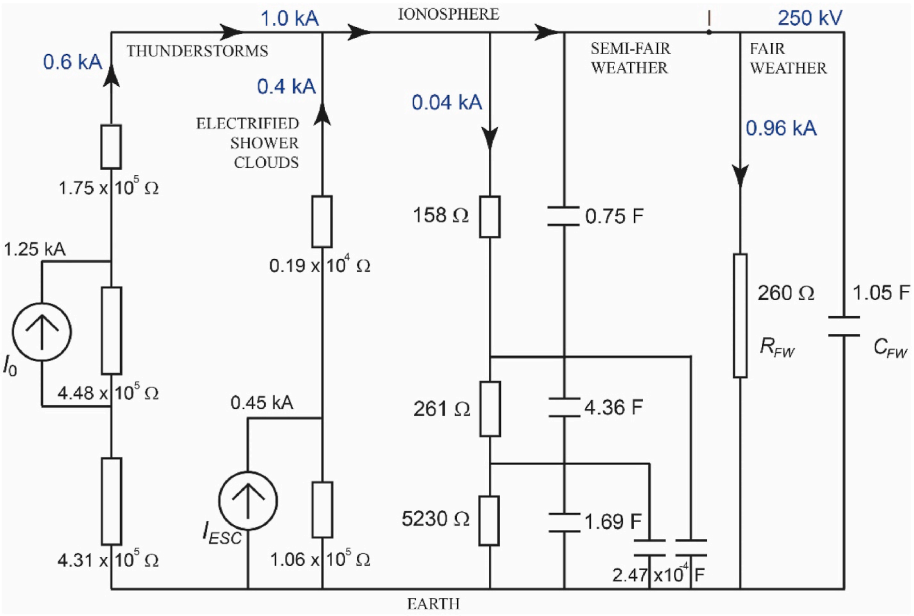

Fig. 5. Schematic diagram of the global electric circuit, including the mutual capacitance of the stratus cloud layer of Harrison et al. (2020), which is 4.36 F.

Further, the air-earth current also showed a maximum at the same time, indicating that the PG pulse was associated with current flow changes (i.e. from the global circuit), rather than local conductivity changes. In addition, the magnitude of the PG variation is about 20%, comparable with the Grímsvötn lightning contribution to the total lightning events observed by ATD. Although not all global lightning will have been captured by ATD, the undetected events will include those with smaller contributions to the global circuit.

After forming 1 min averages of the PG and Grímsvötn lightning flash rate (Fig. 7a), their correlation can be calculated. Fig. 7b shows the lag correlations obtained by displacing the Reading PG values in time. From this, the greatest correlations with the Grímsvötn lightning flash rate are found to be obtained with the PG at Reading about 8–14 min later (Fig. 7b), with a slight maximum at 9 min of lag. These lagged correlations are statistically significant, when evaluated by a method allowing for serial correlation in each dataset (Ebisuzaki, 1997), which would be expected from the known internal magmatic resonances of the volcano and the smoothing effect of the global circuit.

An alternative approach for determining the time constant of the system is to investigate the spectrum of variations present in the PG data, assuming that they were subject to *RC* filtering effect of the global circuit. Fig. 5c shows the amplitude spectrum calculated by Fourier analysis of the data presented in Fig. 4d. Both the lightning flash rate and the PG spectra show a decreasing spectral slope with increasing frequency. However, some of the high frequencies present in the lightning flash rate (at about 0.5 flashes min^{-1}), are not present in the PG, suggesting a damping process to remove them, such as that from the low pass filtering of the global circuit. This can be approximated by a first

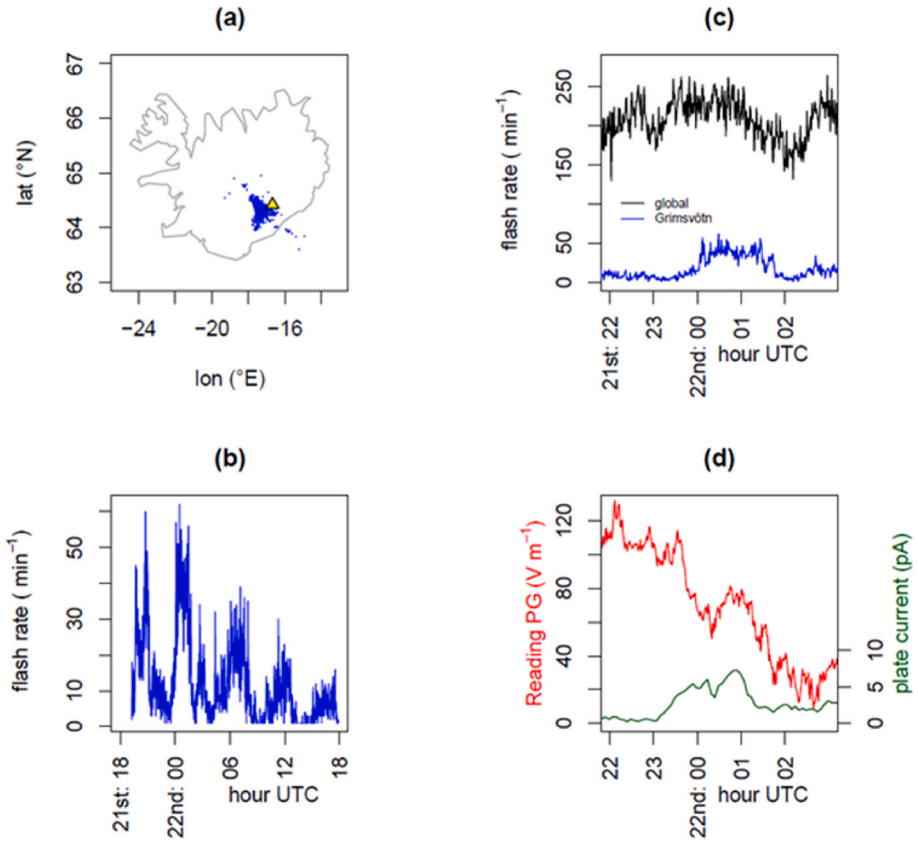

Fig. 6. (a) Lightning events over Iceland detected by Met Office ATD system, on May 21 and 22, 2011 (blue dots), with location of the Grímsvötn volcano also marked (yellow triangle). (b) Time series of all ATD events in the region bounded by 12°W to 27°W, and 61°N to 67°N. (c) Time series of all detected global lightning events (black line), and those over Iceland (blue line) around midnight on May 21, 2011. (d) PG measured at Reading during the same interval as (c), as 1 min averages (red line), and air-earth current measured at an isolated Flat Plate (green line, 5 min averages).

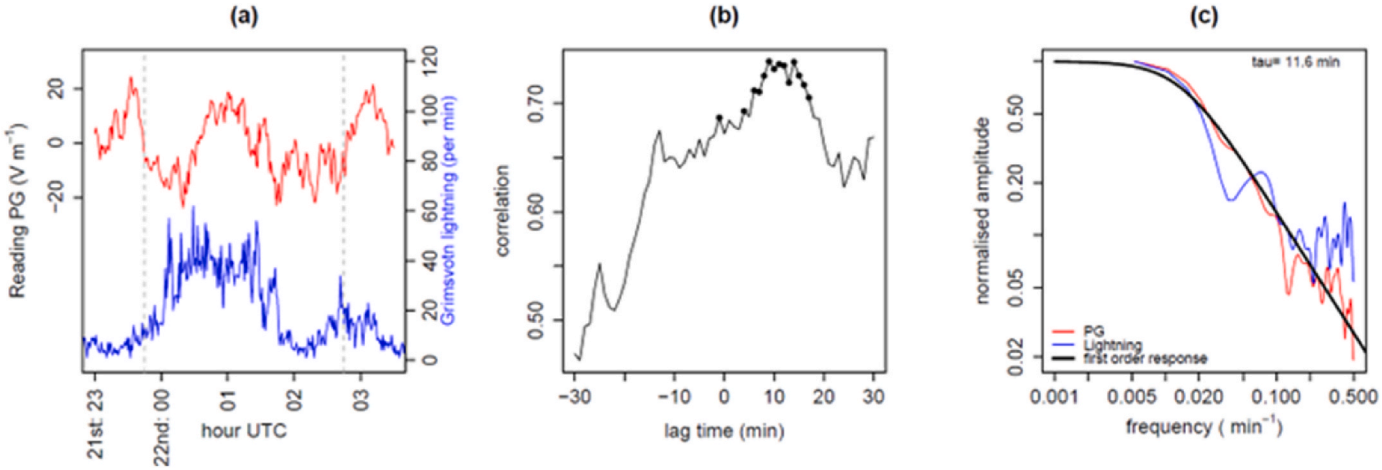

Fig. 7. (a) Time series of Grímsvötn lightning flash rate (blue line, RH axis), and linearly detrended Reading PG (red line, LH axis), for May 2122, 2011, from 1 min averages. (b) Lagged (Spearman) correlation between flash rate and PG, for the interval marked by dashed vertical lines in (a). Points on (b) indicate where the correlations are statistically significant (i.e. probability p of arising by chance, $p < 0.05$), allowing for serial correlation in both time series. (c) Amplitude spectrum of lightning flash rate (blue line) and PG (red line), with a first-order filter response fitted to the PG (thick black line), with the derived time constant, τ, of 11.6 min.

order *RC* filter, which, for a time constant τ, has a relative amplitude response given by

$$V(f) = \frac{1}{\sqrt{1 + 4\pi^2 f^2 \tau^2}} \tag{23}$$

for signals of a frequency f. Fitting the relationship of Eq. (23) to the derived spectrum from the PG (black line in Fig. 7c) gives τ of (11.6 ± 0.2) minutes, where the uncertainty is one standard error. This is within the range of the lag correlations found in Fig. 7b which provides 1 min resolution. The two approaches are therefore not inconsistent, although, as Fig. 7 illustrates, the response of the electronic system is more complicated than that of a simple first order *RC* filter, and therefore the method shown in Fig. 7c is also an approximation.

7. Simulations of the excitation of the global circuit by Grímsvötn lightning

The charging of the global electric circuit by the Grímsvötn lightning can be modelled using the simplified engineering circuits described here. With these, we investigate whether the characteristic increase of the PG at Reading could be explained by the activity of the global circuit, by modelling the characteristic time scales of the variations caused. To simulate the effect of Grímsvötn lightning we perform further simulations of the GEC represented by the circuit shown in Fig. 2 (stratocumulus case), extended by an additional current source due to charging by the volcanic lightning. In our simulation, this time varying current source, I_{0L}(t), adds to the thunderstorm source current I_0 (Fig. 8).

The net effect of the generation of electric current by lightning can be calculated by multiplying the lightning flash rate and the average charge transferred by an average lightning discharge of all produced polarities, Q_L:

$$I_L(t) = \frac{Q_L}{flash\ rate\ (t)} \tag{24}$$

In order to estimate the current source amplitude I_{0L}(t) from the resulting current $I_L(t)$ we need to calculate $R_{2T}/(R_{1T} + R_{2T} + R_{3T}) = 4.48/(4.31 + 4.48{+}0.0175) \cong 0.5$, where R_{1T}, R_{2T}, R_{3T} are the three resistances in the thunderstorm generation region, and use Eq. (25).

$$I_L(t) = \frac{Q_{0L}}{flash\ rate\ (t)} \cong \frac{1}{0.5}\frac{Q_L}{flash\ rate\ (t)} \tag{25}$$

The applied current source I_{0L}(t) is defined to follow the time variation of the Grímsvötn lightning rate, and Q_L is estimated to be about +2.5 Coulombs, in order to account for the rise of the ionospheric potential which should translate into the observed amplitude and the increase of the PG as observed at Reading of the order of 10 Vm^{-1}; exact match of both the amplitude and the increase is difficult, among other effects, due to differences in the conductivity profiles. The prescribed value of +2.5 Coulombs is a fairly feasible value, considering that an average electric charge of several Coulombs can be transferred by lightning discharges (e.g., Rycroft and Odzimek, 2010), even though the exact value and sign of the charge depends on the lightning and cloud polarity. This implies that Q_{0L} should be close to 5 C. Our simulation was performed exactly for $Q_{0L} = 5$ C, and the flash rate in the interval 23:00 UT - 04:00 UT (Fig. 9a). From the transient analysis output the time variation of the electric potentials and currents in this circuit were retrieved. In order to analyse the variation of the potential gradient at ground level in both the fair weather and semi fair weather areas, another alteration to the circuit is needed. An additional node is introduced in the semi fair weather part of the circuit, dividing the lowest resistance 6500 Ω into two parts: one part is the resistance of up to 1 metre above the ground (~3 Ω), and the remaining resistance is the portion up to the cloud base, so the electric potential of this node represents the modelled value of the PG. The value of the resistance between the ground and the node is set to indicate an electric potential difference of ~100 V m^{-1} at the starting point (the Reading PG was about 100 V m^{-1} when the lightning rate began to rise). In a similar manner, such a probe node and resistor are introduced in the fair weather area of the circuit, in order to follow the PG value in the purely fair weather part of the circuit.

The results of these simulations are shown in Fig. 9b and c: these are the variations of the ionospheric potential V_I, the electric potential gradient in semi fair weather region and the PG in fair weather during the simulated interval. In addition, the serial correlation of the lightning current I_{0L} with the simulated PG values was calculated. The correlation started to maximise at the lag time of 3 min for the correlation with the fair weather PG (the potential of node "F"), and at 9 min in case of the semi fair weather PG (potential of node "S", see Fig. 6d). The physical reason for the increased lag time in the semi fair weather area compared to pure fair weather is the separation of the capacitance and resistance of the cloud layer itself from those of the boundary layer below it. Moreover, these two characteristic lag times agree with the lag time determined from observations, as discussed in Section 4 and in this Section, respectively, building confidence in the engineering model of the GEC considered.

Recent results from Bór et al. (2023) further corroborate the timescales derived in this work. These show that intense cloud to ground lightning discharges over the erupting Hunga Tonga volcano on January 15, 2022 impulsively charged the DC GEC, on two separate occasions. Observations of PG changes made near the Earth's surface at six different stations in Europe and the USA during these events showed that

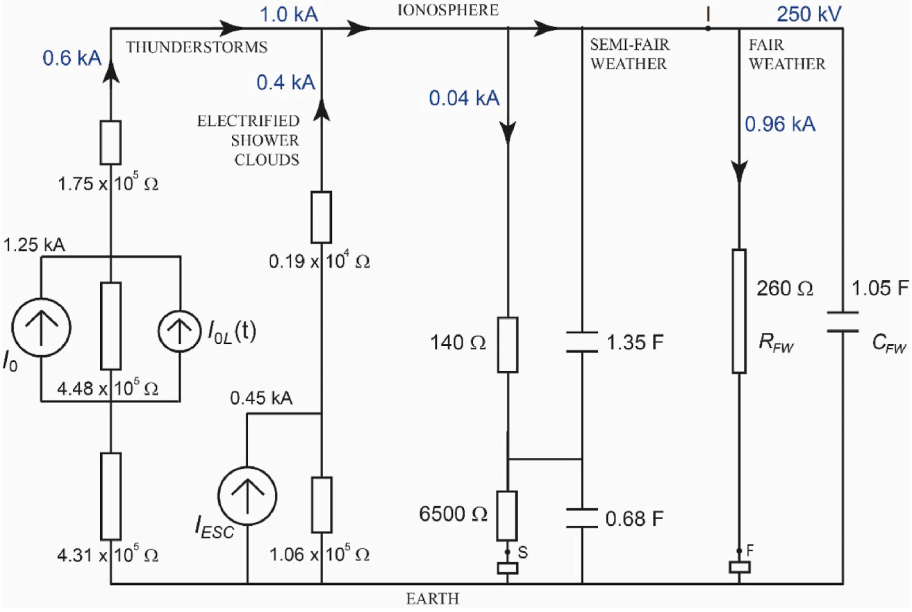

Fig. 8. Schematic diagram of the global electric circuit, with 70% of fair weather area and 30% of semi fair weather area covered by stratocumulus, affected by Grímsvötn lightning represented by current source I_{0L}. Small resistors (with a resistance of several Ohms) in the semi fair weather and fair weather areas probe the ground level electric potential gradient.

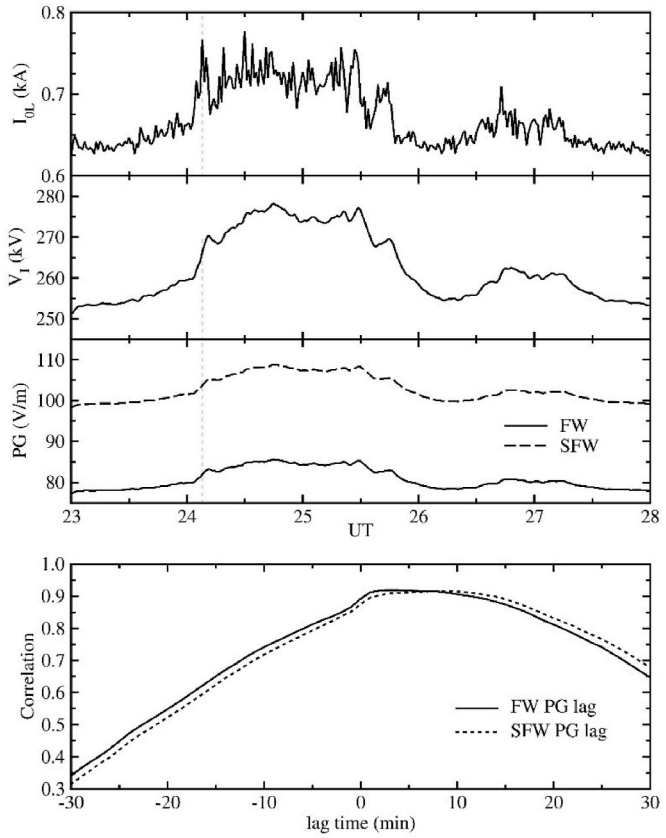

Fig. 9. (a) Lightning current source amplitude. (b) Simulated ionospheric potential. (c) Simulated electric potential gradient in the semi fair weather (SFW) area and purely fair weather (FW) area of the GEC represented by the circuit shown in Fig. 6. (d) Lagged correlation between the model Grímsvötn lightning current source and PG in the fair weather and semi fair weather areas. Gray dashed lines indicate the moment of a maximum in the lightning source amplitude.

the time constant of the GEC is 7–8 min. This coincides with the value derived here for semi-fair weather conditions, which we conclude is effectively the natural state of the system.

8. Discussion of related issues

A further complication is that the situation in the stratus cloud layer, which has been taken to be electrostatic, is actually electrodynamic. The electric charges are moving, and a transfer of charge therefore occurs between the two electrode regions, i.e. an additional non-Ohmic current is present. The electric current density J in the return part of the GEC is 2 pA m^{-2}; it does not depend upon **E**. Such a non-linear system is rather unusual. The force per unit volume of the cloud vapour equals $\rho\,\mathbf{E} + \mathbf{J} \hat{} \mathbf{B}$, where **B** is the geomagnetic field strength, ~40,000 nT. Inserting values from Fig. 5 of Harrison et al. (2020), $\rho = 90$ pC m^{-3} and E = 180 Vm^{-1}, ρ E is 1.6×10^{-8} Nm^{-3}, and the magnitude of the second term = 2 pA $m^{-2} \times 4 \times 10^{-5}$ T = 8×10^{-17} Nm^{-3}. The second term is completely negligible compared with the first. Therefore, effects due to the geomagnetic field do not need to be considered here. Only electric forces, gravitational forces and forces associated with cloud processes (e.g., convection) act on the cloud vapour.

Thunderstorms are believed to be the major source of power for the GEC, but electrified shower clouds are also important (Mach et al., 2011, Lavigne et al., 2017). They are shown as GEC generators on the left hand side of Figs. 1 and 2.

Other interesting ideas on the GEC are presented by Kasemir (2012) in a book devoted to his many studies, with colleagues, over a lifetime (Mazur and Ruhnke, 2012). These include investigations of the charge distribution in a thunderstorm, the mathematics expressing the continuity of current flow when the atmospheric conductivity is given as a function of space and time, the effects of conductivity changes at cloud boundaries, and the effects of turbulence.

Humanity is greatly concerned at present about the increasing concentrations of carbon dioxide in the Earth's atmosphere, currently about 420 parts per million by volume, ppmv, and primarily due to the burning of fossil fuels (Houghton, 2015). Schneider et al. (2019) show that stratocumulus clouds cool the Earth by shading the surface; they predict that these clouds will disappear when CO_2 concentrations rise excessively, to ~1200 ppmv, so causing a marked warming, by ~8 °C. Meehl et al. (2020) have shown that the most recent comprehensive climate models indicate that cloud feedback processes (see, e.g., Yu et al., 2004, Gettelman and Sherwood, 2016, Klein et al., 2017; Zelinka et al., 2020) and cloud-aerosol interactions (Dagan and Stier, 2020) are the most likely contributors to global warming. Liu et al. (2020) have recently discussed the roles of aerosols in affecting climate. We have shown here that cloud-aerosol effects in the lowest 3 km of the atmosphere are crucial in determining the time constant of the global electric circuit. Thus, this region may be where there is a specific linkage between the GEC and climate change if, for example, a property of the clouds (such as their lifetime) is somehow influenced by the electric charge stored on their constituent drops. For example, droplet evaporation can be inhibited by charging (Harrison et al., 2022). There are hints from observations in the polar regions of a global circuit effect on clouds, possibly through such mechanisms (Lavigne and Liu, 2023). Charging occurs where droplets rising in the updraft pass through the conductivity boundary at the cloud base, which is typically ~10 m depth (Tinsley and Zhou, 2012). Updraft speeds of 0.1 ms^{-1} to 1 ms^{-1} will therefore lead to droplets spending 10–100 s in the charging zone. The time constant of the global circuit being significantly longer than this could help facilitate a smoothed and continuous conduction current, leading to more consistent charging of the droplets due to fluctuations being damped out. As mentioned, the stability and breakup of layer clouds is critical to the climate system (Schneider et al., 2019).

9. Conclusions

From the estimates and calculations presented here, we draw the following conclusions.

(i) The representation of the GEC with the upper electrode being the ionosphere, and the capacitance of the fair weather atmosphere depicted in Fig. 1 of Rycroft et al. (2000) as 0.7 F, can now be improved. As shown in Section 2.2, a better electrical analogue is with the upper electrode at a height of only ~3 km, as shown by Haldoupis et al. (2017), so that the capacitance becomes 1.5 F. Therefore, the global time constant of the pure fair weather atmosphere is $RC = 250 \times 1.5 = 375$ s (6.3 min), rather than the earlier value of $250 \times 0.5 = 125$ s (2.1 min) or $250 \times 0.7 = 175$ s (2.9 min) (Rycroft et al., 2000).

(ii) Using the results of Harrison et al. (2020) with 30% of the Earth's surface being covered by stratus clouds at 0.8–1.2 km in height, the capacitance of the fair weather atmosphere over 70% of the Earth's surface is 1.05 F, as shown in Fig. 1. Also included in this representation is the electrical analogue of the semi fair weather stratus clouds. As considered in Section 4, the *RC* time constant of this global electric circuit found using PSpice software is increased to ~497 s (~8.3 min).

(iii) Fig. 2 shows the model GEC including stratocumulus clouds at heights between 2 and 3 km over 30% of the Earth's surface; the global time constant of the GEC becomes ~407 s (~6.8 min).

(iv) Fig. 4 shows the model GEC including stratus clouds at heights between 0.8 and 1.2 km over 25% of the Earth's surface for oceans and 4% over continents; the cloud layer resistances were

calculated using the land and ocean conductivity profiles shown in Fig. 3 the global time constant of this GEC circuit is 480 s (8.0 min).

(v) A new model for the mutual capacitance of the two plates of electrified stratus is presented in Section 5. This is calculated to be 4.36 F; it is shown in Fig. 5 The new value for the global circuit time constant is ~499 s (~8.3 min).

(vi) Experimental studies in atmospheric electricity indicate that comparable time constants occur in the real global circuit, obtained through studies of volcanic lightning observations made during the Grímsvötn and Hunga Tonga eruptions.

(vii) The timescale for semi fair weather PG variations at ground level, derived using Fig. 8 from Grímsvötn observations, is found to be 9 min. This is in accord with the value obtained for the GEC consisting of both fair weather and semi fair weather components, and represents the natural state of the GEC system.

(viii) Existing models of stratocumulus clouds in an atmosphere of ever-increasing amounts of carbon dioxide show that these clouds may eventually disappear altogether. Until then, cloud-aerosol interactions in the lowest 3 km of the atmosphere contribute significantly to global warming; they also determine the time constant of the GEC.

CRediT authorship contribution statement

Michael J. Rycroft: Writing – review & editing, Writing – original draft, Methodology, Formal analysis, Conceptualization. **Anna Odzimek:** Writing – review & editing, Writing – original draft, Visualization, Software, Investigation, Data curation. **R. Giles Harrison:** Writing – review & editing, Writing – original draft, Visualization, Investigation, Data curation.

Declaration of competing interest

The authors declare that they have no known competing financial interests or personal relationships that could have appeared to influence the work reported in this paper.

Data availability

Supporting data is available at https://doi.org/10.18150/CC4ISW.

Acknowledgements

This article has been inspired by collaboration in COST Action CA15211 ELECTRONET: Atmospheric Electricity Network: coupling with the Earth System, climate and biological systems, supported by COST: European Cooperation in Science and Technology.

ATDnet data was provided by the Met Office and can be provided by the Met Office on request.

A. Odzimek acknowledges support from a subsidy from the Ministry of Education and Science to the Institute of Geophysics of the Polish Academy of Sciences.

We are most grateful to Brian Tinsley for his reviewer comments and for the explanation developed in the Appendix. We also appreciate the comments of a further anonymous reviewer.

Appendix

The approximately consistent total load capacitance of ~1.5 F modelled in the different situations described can be understood from the electrostatic theorem stating: "If the potential difference V between the electrodes of a capacitor and the charge on the electrodes Q is fixed, then the capacitance $C = Q/V$ is independent of the distribution (or absence) of space charge between the electrodes, and is also independent of the inter-electrode spacing". For a theoretical capacitor having a vacuum between the electrodes this indicates there is zero space charge contained, with + Q and -Q on the two electrodes. This follows from Gauss's Law

$$\frac{dE}{dz} = \frac{\rho}{\epsilon} \tag{A1}$$

where ρ is the space charge in unit volume and ϵ the permittivity. Considering E_2 and E_1 as the electric fields at the upper and lower boundaries respectively,

$$E_2 - E_1 = \int \frac{dE}{dz} dz = \frac{1}{\epsilon} \int \rho dz \tag{A2}$$

where the integrals are taken from the lower to upper boundary. The space charge in a unit area column from the surface to the upper boundary is

$$q = \int \rho dz \tag{A3}$$

For the global circuit, there is -Q on the land and ocean surface, and + Q distributed between the surface and the upper boundary. The + Q is associated with ions in clear air, ions and dust in the boundary layer, or ions, aerosols and droplets in clouds. E_1 can be considered as the electric field at the surface of the planet in non-generator regions; E_2 is the electric field at the upper boundary, which is zero. Hence $q = -\epsilon E_1$ and the total charge Q in the non-generator area A of the global circuit is given by $Q = qA = -\epsilon A E_1$ which is equal and opposite to the charge on the surface. Inserting numerical values, and taking an average value for E_1 of 130 Vm^{-1} (Harrison, 2013), the magnitude of Q is obtained as 6.17×10^5C, in good agreement with the values in the paper.

Footnotes

[1] http://physics.stackexchange.com/questions/187139/capacitance-of-a-single-charged-plate

[2] http://physics.stackexchange.com/questions/102076/capacitance-of-bodies-with-different-charge

References

Anisimov, S.V., Galichenko, S.V., Prokhorchuk, A.A., Aphinogenov, K.V., 2020. Mid-latitude convective boundary-layer electricity: a study by large-eddy simulation. Atmos. Res. 244, 105035 https://doi.org/10.1016/j.atmosres.2020.105035.

Aplin, K.L., Bennett, A.J., Harrison, R.G., Houghton, I.M.P., 2016. Electrostatics and in situ sampling of volcanic plumes. In: Mackie, S., Cashman, C., Ricketts, H., Rust, A. (Eds.), Volcanic Ash: Hazard Observation and Monitoring. Elsevier.

Aplin, K.L., Harrison, R.G., Rycroft, M.J., 2008. Investigating Earth's atmospheric electricity: a role model for planetary studies. Space Sci. Rev. 137, 11–27. https://doi.org/10.1007/s11214-008-9372-x.

Arason, Þ., Björnsson, H., Petersen, G.N., Roberts, M.J., Collins, M., 2012. Eruptive flow rate resonance during the Grímsvötn 2011 volcanic eruption in Iceland. European Geosciences Union. http://meetingorganizer.copernicus.org/EGU2012/EGU2012-9597.pdf.

Barbosa, S., 2020. Ambient radioactivity and atmospheric electric field: a joint study in an urban environment. J. Environ. Radioactiv. 219, 106283 https://doi.org/10.1016/j.jenvrad.2020.106283.

Baumgaertner, A.J.G., Thayer, J.P., Neely III, R.R., Lucas, G., 2013. Toward a comprehensive global electric circuit model: atmospheric conductivity and its variability in CESM1(WACCM) model simulations. J. Geophys. Res. Atmos. 118, 9221–9232. https://doi.org/10.1002/jgrd.50725.

Bayona, V., Flyer, N., Lucas, G.M., Baumgaertner, A.J.G., 2015. A 3-D RBF-FD solver for modeling the atmospheric global electric circuit with topography (GEC-RBFFD v1.0). Geosci. Model Dev. (GMD) 8, 3007–3020. https://doi.org/10.5194/gmd-8-3007-2015.

Bór, J., Bozóki, T., Sátori, G., Williams, E., Behnke, S.A., Rycroft, M.J., Buzás, A., Silva, H.G., Kubicki, M., Said, R., Vagasky, C., Steinbach, P., Szabóné André, K., Atkinson, M., 2023. Responses of the AC/DC global electric circuit to volcanic electrical activity in the Hunga Tonga - Hunga Ha'apai eruption on 15 January 2022. J. Geophys. Res. Atmos. 128, e2022JD038238 https://doi.org/10.1029/2022JD038238.

Bennett, A.J., Gaffard, C., Nash, J., Callaghan, G., Atkinson, N.C., 2011. The effect of modal interference on VLF long-range lightning location networks using the waveform correlation technique. J. Atmos. Ocean. Tech. 28 (8), 993–1006. https://doi.org/10.1175/2011JTECHA1527.1.

Brown, R., 1973. Ionospheric effects of cosmic γ-ray bursts. Nature 246, 83–84. https://doi.org/10.1038/246083a0.

Cohen, C.M.S., Mewaldt, R.A., 2018. The ground-level enhancement event of September 2017 and other large solar energetic particle events of cycle 24. Space Weather 16 (10), 1616–1623. https://doi.org/10.1029/2018SW002006.

Dagan, G., Stier, P., 2020. Ensemble daily simulations for elucidating cloud-aerosol interactions under a large spread of realistic environmental conditions. Atmos. Chem. Phys. 20, 6291–6303. https://doi.org/10.5194/acp-20-6291-2020.

Ebisuzaki, W., 1997. A method to estimate the statistical significance of a correlation when the data are serially correlated. J. Clim. 10 (9), 2147–2153. https://doi.org/10.1175/1520-0442(1997)010<2147:AMTETS>2.0.CO, 2.

Füllekrug, M., Nnadih, S., Soula, S., Mlynarczyk, J., Stock, M., Lapierre, J., Kosch, M., 2019. Maximum sprite streamer luminosity near the stratopause. Geophys. Res. Lett. 46 (21), 12572–12579. https://doi.org/10.1029/2019GL084331.

Füllekrug, M., Mareev, E.A., Rycroft, M.J. (Eds.), 2006. Sprites, Elves and Intense Lightning Discharges. Springer, Netherlands, Dordrecht. https://doi.org/10.1007/1-4020-4629-4.

Gettelman, A., Sherwood, S.C., 2016. Processes responsible for cloud feedback. Curr. Clim. Change Rep. 2, 179–189. https://doi.org/10.1007/s40641-016-0052-8.

Golubenko, K., Rozanov, E., Mironova, I., Karagodin, A., Usoskin, I., 2020. Natural sources of ionization and their impact on atmospheric electricity. Geophys. Res. Lett. 47, e2020GL088619 https://doi.org/10.1029/2020GL088619.

Gray, L.J., Beer, J., Geller, M., Haigh, J.D., Lockwood, M., Matthes, K., Cubasch, U., Fleitmann, D., Harrison, G., Hood, L., Luterbacher, J., Meehl, G.A., Shindell, D., van Geel, B., White, W., 2010. Solar influences on climate. Rev. Geophys. 48 https://doi.org/10.1029/2009RG000282.

Haldoupis, C., Rycroft, M., Williams, E., Price, C., 2017. Is the "Earth-ionosphere capacitor" a valid component in the atmospheric global electric circuit? J. Atmos. Sol. Terr. Phys. 164, 127–131. https://doi.org/10.1016/j.jastp.2017.08.012.

Harrison, R., 2006. Urban smoke concentrations at Kew, London, 1898-2004. Atmos. Env. 40, 3327–3332. https://doi.org/10.1016/j.atmosenv.2006.01.042.

Harrison, R.G., 2013. The Carnegie curve. Surv. Geophys. 34, 209–232. https://doi.org/10.1007/s10712-012-9210-2.

Harrison, R.G., 2020. Behind the curve: a comparison of historical sources for the Carnegie curve of the global atmospheric electric circuit. Hist. Geo. Space Sci. 11, 207–213. https://doi.org/10.5194/hgss-11-207-2020.

Harrison, R.G., Aplin, K.L., Rycroft, M.J., 2010. Atmospheric electricity coupling between earthquake regions and the ionosphere. J. Atmos. Sol. Terr. Phys. 72, 376–381. https://doi.org/10.1016/j.jastp.2009.12.004.

Harrison, R.G., Nicoll, K.A., Mareev, E., Slyunyaev, N., Rycroft, M.J., 2020. Extensive layer clouds in the global electric circuit: their effects on vertical charge distribution and storage. Proc. Roy. Soc. A 476, 20190758. https://doi.org/10.1098/rspa.2019.0758.

Harrison, R.G., Marlton, G.J., Ambaum, M.H.P., Nicoll, K.A., 2022. Modifying natural droplet systems by charge injection. Phys. Rev. Res. 4, L022050 https://doi.org/10.1103/PhysRevResearch.4.L022050.

Hayakawa, M., 2015. Earthquake Prediction with Radio Techniques. John Wiley & Sons, Singapore. https://doi.org/10.1002/9781118770368.

Hess, M., Koepke, P., Schult, 1998. Optical properties of aerosols and clouds: the software package OPAC. Bull. Amer. Meteorol. Soc. 79, 831–844. https://doi.org/10.1175/1520-0477(1998)079<0831:OPOAAC>2.0.CO;2.

Holzer, R.E., Saxon, D.S., 1952. Distribution electrical conduction currents in the vicinity of thunderstorms. J. Geophys. Res. 57 (2), 207–216. https://doi.org/10.1029/JZ057i002p00207.

Houghton, J., 2015. Global Warming: the Complete Briefing, fifth ed. Cambridge University Press. https://doi.org/10.1017/CBO9781316134245.

Hunting, E.R., Matthews, J., de Arróyabe Hernáez, P.F., England, S.J., Kourtidis, K., Koh, K., Nicoll, K., Harrison, R.G., Manser, K., Price, C., Dragovic, S., Cifra, M., Odzimek, A., Robert, D., 2020. Challenges in coupling atmospheric electricity with biological systems. Int. J. Biometeorol. 65, 45–58. https://doi.org/10.1007/s00484-020-01960-7.

Inan, U.S., Lehtinen, N.G., Lev-Tov, S.J., Johnson, M.P., Bell, T.F., Hurley, K., 1999. Ionization of the lower ionosphere by γ-rays from a Magnetar: detection of a low energy (3-10 keV) component. Geophys. Res. Lett. 26 (22), 94–8276. https://doi.org/10.1029/1999GL010690.

Kasemir, H.W., 2012. See: Mazur and Ruhnke, 2012.

Klein, S.A., Hartmann, D.L., 1993. The seasonal cycle of low stratiform clouds. J. Clim. 6, 1587–1606. https://doi.org/10.1175/1520-0442(1993)006<1587:TSCOLS>2.0.CO, 2.

Klein, S.A., Hall, A., Norris, J.R., Pincus, R., 2017. Low-cloud feedbacks from cloud-controlling factors: a review. Surv. Geophys. 38, 1307–1329. https://doi.org/10.1007/s10712-017-9433-3.

Kubicki, M., Odzimek, A., Neska, M., 2016. Relationship of ground-level aerosol concentration and atmospheric electric field at three observation sites in the Arctic, Antarctic and Europe. Atmos. Res. 178–179, 329–346. https://doi.org/10.1016/j.atmosres.2016.03.029.

Kudintseva, I., Nickolaenko, A., Rycroft, M.J., Odzimek, A., 2016. AC and DC global electric circuit properties and the height profile of atmospheric conductivity. Ann. Geophys. Italy 59 (5), A0545. https://doi.org/10.4401/ag-6870.

Lavigne, T., Liu, C., 2023. Relationships among diurnal variations of polar night cloud, precipitation, surface temperatures, and the fair-weather return current of the global electric circuit. J. Atmos. Sol. Terr. Phys. 244, 106026 https://doi.org/10.1016/j.jastp.2023.106026.

Lee, A.C.L., 1986. An operational system for the remote location of lightning flashes using a VLF arrival time difference technique. J. Atmos. Ocean. Tech. 3 (4) https://doi.org/10.1175/1520-0426(1986)003<0630:aosftr>2.0.co;2, 630-624.

Liu, L., Cheng, Y., Wang, S., Wei, C., Pöhlker, M., Pöhlker, C., Artaxo, P., Shrivastava, M., Andreae, M.O., Pöschl, U., Su, H., 2020. Impact of biomass burning aerosols on radiation, clouds, and precipitation over the Amazon during the dry season: dependence of aerosol-cloud and aerosol-radiation interactions on aerosol loading. Atmos. Chem. Phys. Discuss. 2020 https://doi.org/10.5194/acp-2020-191.

Mach, D.M., Blakeslee, R.J., Bateman, M.G., 2011. Global electric circuit implications of combined aircraft storm electric current measurements and satellite-based diurnal lightning statistics. J. Geophys. Res. 116, D05201 https://doi.org/10.1029/2010JD014462.

Mailyan, B.G., Nag, A., Dwyer, J.R., 2020. Gamma-ray and radio-frequency radiation from thunderstorms observed from space and ground. Sci. Rep. 10, 7286. https://doi.org/10.1038/s41598-020-63437-2.

Makino, M., Ogawa, T., 1985. Quantitative estimation of global circuit. J. Geophys. Res. 90 (D4), 5961–5966. https://doi.org/10.1029/JD090iD04p05961.

Markson, R., 2007. The global circuit intensity: its measurement and variation over the last 50 years. Bull. Am. Met. Soc. 88, 1–19. https://doi.org/10.1175/BAMS-88-2-223.

Mazur, V., Ruhnke, L.H. (Eds.), 2012. Heinz Wolfram Kasemir: His Collected Works. https://doi.org/10.1002/9781118704813.ch49.

Meehl, G.A., Senior, C.A., Eyring, V., Flato, G., Lamarque, J.F., Stouffer, R.J., Taylor, K.E., Schlund, M., 2020. Context for interpreting equilibrium climate sensitivity and transient climate response from the CMIP6 Earth system models. Sci. Adv. 6 (26) https://doi.org/10.1126/sciadv.aba1981.

Mühleisen, R., 1976. The Global circuit and its parameters. In: Dolezalek, H., Reiter, R., Landsberg, H.E. (Eds.), Electrical Processes in Atmospheres. Steinkopff, pp. 467–476. https://doi.org/10.1007/978-3-642-85294-7_73.

Odzimek, A., Baranski, P., Kubicki, M., Jasinkiewicz, D., 2018. Electrical signatures of Nimbostratus and Stratus clouds in ground-level vertical atmospheric electric field and current density at mid-latitude station Swider, Poland. Atmos. Res. 209, 188–203. https://doi.org/10.1016/j.atmosres.2018.03.018.

Odzimek, A., Lester, M., Kubicki, M., 2010. Egatec - a new high-resolution engineering model of the global atmospheric electric circuit. 1. Currents in the lower atmosphere. J. Geophys. Res. Atmos. 115, D18207 https://doi.org/10.1029/2009JD013341.

Ouzounov, D., Pulinets, S., Liu, J.Y., Hattori, K., Han, P., 2018. Multiparameter assessment of pre-earthquake atmospheric signals. In: Ouzounov, D., Pulinets, S., Hattori, K., Taylor, P. (Eds.), Pre-Earthquake Processes: A Multidisciplinary Approach to Earthquake Prediction Studies. American Geophysical Union, pp. 339–359. https://doi.org/10.1002/9781119156949.ch20 (Chapter 20).

Palmer, S.J., Rycroft, M.J., Cermack, M., 2006. Solar and geomagnetic activity, extremely low frequency magnetic and electric fields and human health at the Earth's surface. Surv. Geophys. 27 (5), 557–595. https://doi.org/10.1007/s10712-006-9010-7.

Peterson, M., Deierling, W., Liu, C., Mach, D., Kalb, C., 2017. A TRMM/GPM retrieval of the total mean generator current for the global electric circuit. J. Geophys. Res. Atmos. 122 (18), 10025–10049. https://doi.org/10.1002/2016JD026336.

Ponomarev, E.A., Cherneva, N.V., Firstov, P.P., 2011. Formation of a local atmospheric electric field. Geomagn. Aeron. 51, 402–408. https://doi.org/10.1134/S0016793211030145.

Price, C., Harrison, G., Rycroft, M.J., 2015. Impact of solar variability on the global electric circuit. In: Dudok de Wit, K., et al. (Eds.), Earth's Climate Response to a Changing Sun, COST Action ES1005. EDP Sciences, pp. 281–288.
Price, C., Penner, J., Prather, M., 1997. NOx from lightning, 2: constraints from the global atmospheric electric circuit. J. Geophys. Res. Atmos. 102, 5943–5951. https://doi.org/10.1029/96JD02551.
Pulinets, S., Davidenko, D., 2014. Ionospheric precursors of earthquakes and global electric circuit. Adv. Space Res. 53 (5), 709–723. https://doi.org/10.1016/j.asr.2013.12.035.
Rycroft, M.J., Harrison, R.G., 2012. Electromagnetic atmosphere-plasma coupling: the global atmospheric electric circuit. Space Sci. Rev. 168, 363–384. https://doi.org/10.1007/s11214-011-9830-8.
Rycroft, M.J., Harrison, R.G., Nicoll, K.A., Mareev, E.A., 2008. An overview of Earth's global electric circuit and atmospheric conductivity. Space Sci. Rev. 137, 83–105. https://doi.org/10.1007/s11214-008-9368-6.
Rycroft, M.J., Israelsson, S., Price, C., 2000. The global atmospheric electric circuit, solar activity and climate change. J. Atmos. Sol. Terr. Phys. 62 https://doi.org/10.1016/S1364-6826(00)00112-7, 1563-157.
Rycroft, M.J., Nicoll, K.A., Aplin, K.L., Harrison, R.G., 2012. Recent advances in global electric circuit coupling between the space environment and the troposphere. J. Atmos. Sol. Terr. Phys. 90–91, 198–211. https://doi.org/10.1016/j.jastp.2012.03.015.
Rycroft, M.J., Odzimek, A., 2010. Effects of lightning and sprites on the ionospheric potential, and threshold effects on sprite initiation, obtained using an analog model of the global atmospheric electric circuit. J. Geophys. Res. Space 115, A00E37. https://doi.org/10.1029/2009JA014758.
Rycroft, M.J., Odzimek, A., Arnold, N.F., Fullekrug, M., Kulak, A., Neubert, T., 2007. New model simulations of the global atmospheric electric circuit driven by thunderstorms and electrified shower clouds: the roles of lightning and sprites. J. Atmos. Sol. Terr. Phys. 69, 2485–2509. https://doi.org/10.1016/j.jastp.2007.09.004.
Schneider, T., Kaul, C.M., Pressel, K.G., 2019. Possible climate transitions from breakup of stratocumulus decks under greenhouse warming. Nat. Geosci. 12, 163–167. https://doi.org/10.1038/s41561-019-0310-1.
Schonland, B.F.J., 1932. Atmospheric Electricity, first ed. Methuen and Co., London.
Siingh, D., Gopalakrishnan, V., Singh, R.P., Kamra, A.K., Singh, S., Pant, V., Singh, R., Singh, A.K., 2007. The atmospheric global electric circuit: an overview. Atmos. Res. 84, 91–110. https://doi.org/10.1016/j.atmosres.2006.05.005.
Siingh, D., Singh, R.P., Singh, A.K., Kulkarni, M.N., Gautam, A.S., Singh, A.K., 2011. Solar activity, lightning and climate. Surv. Geophys. 32, 659. https://doi.org/10.1007/s10712-011-9127-1.
Siingh, D., Singh, R.P., Kumar, S., Dharmaraja, T., Singh, Abhay K., Singh, Ashok K., Patil, M.N., Singh, S., 2015. Lightning and middle atmospheric discharges in the atmosphere. J. Atmos. Sol. Terr. Phys. 134, 78–101. https://doi.org/10.1016/j.jastp.2015.10.001.
Tacza, J., Raulin, J.P., Macotela, E., Marun, A., Fernandez, G., Bertoni, F., Lima, L., Samanes, J., Buleje, Y., Correia, E., Alves, G., Makita, K., 2020. Local and global effects on the diurnal variation of the atmospheric electric field in South America by comparison with the Carnegie curve. Atmos. Res. 240, 104938 https://doi.org/10.1016/j.atmosres.2020.104938.
Tinsley, B.A., 2022. Uncertainties in evaluating global electric circuit interactions with atmospheric clouds and aerosols, and consequences for radiation and dynamics. J. Geophys. Res. Atmos. 127, e2021JD035954 https://doi.org/10.1029/2021JD035954.
Tinsley, B.A., Zhou, L., 2006. Initial results of a global circuit model with variable stratospheric and tropospheric aerosols. J. Geophys. Res. 111, D16205 https://doi.org/10.1029/2005JD006988.
Tinsley, B.A., Zhou, L., 2012. Time dependent charging of layer clouds in the global electric circuit. Adv. Space Res. 50 (2012), 828–842. https://doi.org/10.1016/j.asr.2011.12.018.
Uman, M.A., 1974. The Earth and its atmosphere as a leaky spherical capacitor. Am. J. Phys. 42, 1033–1034. https://doi.org/10.1119/1.1987924.
Williams, E., Mareev, E., 2014. Recent progress on the global electrical circuit. Atmos. Res. 135–136, 208–227. https://doi.org/10.1016/j.atmosres.2013.05.015.
Wilson, C.T.R., 1921. Investigation on lightning discharges and on the electric field of thunderstorms. Phil. Trans. Roy. Soc. Lond. 211, 73–115. https://doi.org/10.1098/rsta.1921.0003.
Wilson, C.T.R., 1924. Investigation on lightning discharges and on the electric field of thunderstorms. Proc. Phys. Soc., London 37, 32D–37D. https://doi.org/10.1088/1478-7814/37/1/314.
Wilson, C.T.R., 1929. Some thunderstorm problems. J. Franklin Inst. 208, 1–12. https://doi.org/10.1016/S0016-0032(29)90935-2.
Yu, R., Wang, B., Zhou, T., 2004. Climate effects of the deep continental Stratus clouds generated by the Tibetan Plateau. J. Clim. 17, 2702–2713. https://doi.org/10.1175/1520-0442(2004)017<2702:CEOTDC>2.0.CO, 2.
Zelinka, M.D., Myers, T.A., McCoy, D.T., Po-Chedley, S., Caldwell, P.M., Ceppi, P., Klein, S.A., Taylor, K.E., 2020. Causes of higher climate sensitivity in CMPIP6 models. Geophys. Res. Lett. 47, e2019GL085782 https://doi.org/10.1029/2019GL085782.
Zhou, L.M., Tinsley, B.A., 2010. Global circuit model with clouds. J. Atmos. Sci. 67, 1143–1156. https://doi.org/10.1175/2009JAS3208.1.
Surkov, V.V., Hayakawa, M., 2020. Progress in the Study of Transient Luminous and Atmospheric Events: A Review. Surv Geophys 41, 1101–1142. https://doi.org/10.1007/s10712-020-09597-2.
Harrison, R.G., Aplin, K.L., Rycroft, M.J., 2014. Brief Communication: Earthquake–cloud coupling through the global atmospheric electric circuit. Nat. Hazards Earth Syst. Sci. 14, 773–777. https://doi.org/10.5194/nhess-14-773-2014.